Automotive Science and Engineering, Vol. 12, No. 2, (2022), 3827-3837

Iran University of Science and Technology

Automotive Science and Engineering

Journal Homepage: ase.iust.ac.ir

ISSN: 2008-9899

Chaotic Study along with Comparison of Chaotic Control Algorithms in Active Suspension System

Yavar Nourollahi Golouje[1], Seyyed Mahdi Abtahi[1*], Majid Majidi[1]

[1]Department of Mechanical Engineering, Faculty of Industrial and Mechanical Engineering, Qazvin Branch, Islamic Azad University, Qazvin, Iran

ARTICLE INFO

Article history:
Received: 6 Mar 2022
Accepted: 11 Jun 2022
Published: 11 Jun 2022

Keywords:
Bifurcation diagram
Lyapunov exponent
Chaos control
fast terminal sliding mode
Pyragas algorithm
Fuzzy logic

A B S T R A C T

In this work, analysis and control of the chaotic oscillations in bounce dynamic of vehicle have been studied according to the comparison of controller based on the nonlinear control and chaos controller on the basis of the chaotic system properties. After modeling the vehicle dynamic, the chaotic behavior of the uncontrolled system was determined using combination of the numerical analysis including bifurcation diagrams and max Lyapunov exponent. The system parameters values were then identified in the quasi-periodic and chaotic behavior system. To eliminate the chaos, the control signal was first developed using a nonlinear fast-terminal sliding mode control algorithm that its control coefficients are online estimated by fuzzy logic which was designed for vehicle vertical dynamics. Then the delayed feedback control was designed on the basis of developed Pyragas scheme to control the system based on the properties of the chaotic vehicle system and generation of a small control signal. Comparison of the feedback system depicts priority of the Fuzzy-Pyragas controller in less energy consumption and better behavior.

1. Introduction

There are two chaos controller approaches to eliminate the chaotic oscillations. First, the chaotic dynamics is considered as a nonlinear system and common nonlinear controller is used for chaos nonlinear systems such as sliding mode controller (SMC) as a robust control in addition to ensure the stability of the closed loop system. Also SMC has proper performance in dealing with uncertainties in the system modeling. Another approach for controlling of chaotic systems is to use the properties of chaos in the control algorithm, including the Ott-Grebogi-Yorke (OGY) method based on Poincaré map, which was introduced in 1990. OGY can stabilize the unstable periodic orbits (UPOs) with a small control signal that orbits lead to the equilibrium point or stable cycle circuit. The main problem of the OGY method is the exact mathematical solution of the chaotic orbits. But, the Pyragas proposed a simple and efficient method based on Delayed Feedback Control (DFC) to stabilize the UPOs without their exact solutions. In the Pyragas controller,

*Corresponding Author
Email Address: m.abtahi@qiau.ac.ir
https://doi.org/10.22068/ase.2022.609

a UPO is generally estimated by a time delay mode. In order to achieve a small control signal, ergodicity property of the chaotic systems is used to reduce energy consumption besides the better performance in less time [1-4].

Due to the nonlinear nature of the vibrating elements of the suspension system such as springs and dampers, the vehicle vertical dynamics have a nonlinear structure. Therefore, it is possible to occur the quasi-periodic and chaotic responses in the dynamics for some values of system parameters and the force applied to the vehicle wheels by the roughness of the road surface [5-6]. Recently, many studies have been conducted on the analysis of chaotic dynamics as well as the chaos control of vehicle vibrations. Zhou and Ishitobi [7] studied the analysis of bifurcation and chaos in a half-vehicle model. They studied the effect of damping coefficient on the vehicle nonlinear dynamic behavior and showed that chaotic behavior occurs in the modeled vehicle under the road surface force. Also, the vehicle chaos dynamics was analyzed and controlled with a semi-active suspension system by optimally discrete OGY chaos control [8]. For doing so, the phase portrait trajectories and Poincaré section tools are used and the results of OGY chaos control compared to nonlinear controllers depicted a decrease in settling time in the responses as well as the size of the control input signal and energy consumption [9].

In this work, after mathematical modeling, the chaos is studied via the bifurcation diagrams and Lyapunov exponent and the quasi-periodic and chaotic behavior system can be determined. Then, by presenting the fuzzy system for the fast-terminal SMC and the extended Pyragas, the control systems are designed to eliminate chaos in the bounce model. As a result, by development of fast terminal SMC while using exponential sliding surface, the trajectories of the feedback system can be fast stabilized. Also, in the Pyragas method, the SMC algorithm is integrated with this control method, which innovatively fuzzy inference is used to estimate the control gains of the sliding delay feedback system. Integration of fuzzy in the control strategies can eliminate the chatting that is created by the sliding of the trajectories around the sliding surface and leads to faster convergence. The simulation control results demonstrate the better performance of extended Pyragas control system compared to the fast terminal SMC in reducing the stabilization time and energy consumption of the system.

2. Dynamical Modeling

Figure 1 shows a dynamic model of half-vehicle model, in which the vehicle is modeled as a sprung mass with two degrees of freedom including vertical displacement (x_b) and rotation about the transverse axis of the body (θ) along with the two non-suspended masses of the front and rear tires model.

Suspension system is modeled as nonlinear spring and damper. Also, the actuators forces in front and rear active suspension are u_f and u_r respectively. The mathematical relation governing the force of nonlinear springs and dampers of the suspension system is expressed as follows [7]

$$f_s = k_s \,\mathrm{sgn}(\Delta_s)|\Delta_s|^n \tag{1}$$

$$f_{sc} = c_s \Delta \dot{x}_s \tag{2}$$

Displacement of input excitation from the road surface is assumed as sinusoidal function, which is modeled as follows:

$$X_{fd} = A\sin(\Omega t) = A\sin(2\pi f t) \tag{3}$$

$$X_{rd} = A\sin(\Omega t + \alpha) = A\sin(2\pi f t + \alpha) \tag{4}$$

, where A and f are the amplitude and frequency of the excitation force and α represents the time delay related to the roughness of the road surface between the front and rear tires.

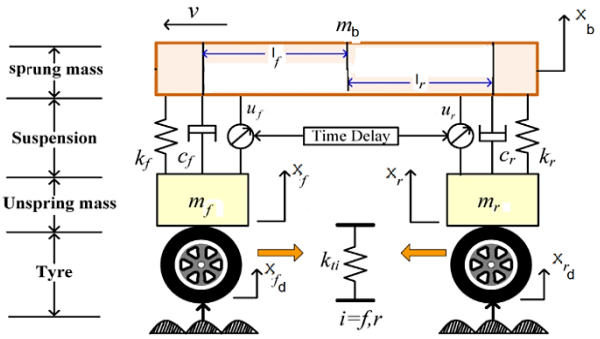

Figure 1: Half vehicle model with active suspension under road surface roughness

Using Newton-Euler laws, dynamical equations of the vertical model in vehicle are obtained as follows.

$$\begin{aligned} M_b \ddot{X}_b = & -k_{f2}\,\mathrm{sgn}(\Delta_{bf2})|\Delta_{bf2}|^{n_{f2}} - c_{f2}\dot{\Delta}_{bf2} \\ & - k_{r2}\,\mathrm{sgn}(\Delta_{br2})|\Delta_{br2}|^{n_{r2}} - c_{r2}\dot{\Delta}_{br2} \\ & - M_b g + u_f + u_r \end{aligned} \quad (5)$$

$$\begin{aligned} J\ddot{\theta} = & \left[\begin{matrix} k_{f2}\,\mathrm{sgn}(\Delta_{bf2})|\Delta_{bf2}|^{n_{f2}} \\ +c_{f2}\dot{\Delta}_{bf2} - u_f \end{matrix}\right] l_f \cos\theta \\ & - \left[\begin{matrix} k_{r2}\,\mathrm{sgn}(\Delta_{br2})|\Delta_{br2}|^{n_{r2}} \\ +c_{r2}\dot{\Delta}_{br2} - u_r \end{matrix}\right] l_r \cos\theta \end{aligned} \quad (6)$$

$$\begin{aligned} M_f \ddot{X}_f = & k_{f2}\,\mathrm{sgn}(\Delta_{bf2})|\Delta_{bf2}|^{n_{f2}} \\ & + c_{f2}\dot{\Delta}_{bf2} \\ & - k_{f1}\,\mathrm{sgn}(\Delta_{bf1})|\Delta_{bf1}|^{nf1} \\ & - c_{f1}\dot{\Delta}_{bf1} - M_f g + u_f \end{aligned} \quad (7)$$

$$\begin{aligned} M_r \ddot{X}_r = & k_{r2}\,\mathrm{sgn}(\Delta_{br2})|\Delta_{br2}|^{n_{r2}} \\ & + c_{r2}\dot{\Delta}_{br2} \\ & - k_{r1}\,\mathrm{sgn}(\Delta_{br1})|\Delta_{br1}|^{nr1} \\ & - c_{r1}\dot{\Delta}_{br1} - M_r g + u_r \end{aligned} \quad (8)$$

3. Chaos Analysis

Numerical simulations of the dynamical system based on the equations (5)-(8) have been done using the fourth-order Runge-Kutta method. The numerical values of the various parameters in the simulation are expressed according to Table 1. The values of these parameters, which change the qualitative nature of the system motion, are referred to as critical values in bifurcation diagrams. The distinction between periodic and chaotic behavior is made by studying the bifurcation shapes.

Table 1: Numerical values of system parameters

System parameters	Values
Mb	1180 kg
J	6336kgm^2
Mf	50kg
Mr	45kg
kf2	36952N/m
kr2	30130 N/m
kf1 , kr1	140000N/m
cf2u , cf2r	500kg/s
cf2d , cfr2	360kg/s
nr2 nf2	1.5
nr1 , nf1	1.25
lf	1.123m
lr	1.377m

Figure 2 demonstrates the bifurcation diagram of the state variables relative to the changes of the control parameter of the road surface excitation amplitude, which are plotted in the range $0 \le A \le 0.2$m . The results of Fig. 2 depict that almost in $0.05 \le A \le 0.014$, there is an irregular dynamic behavior with the occurrence of chaos. By increasing the amplitude value after the mentioned range, the bifurcation diagram shows regular and periodic dynamic behavior.

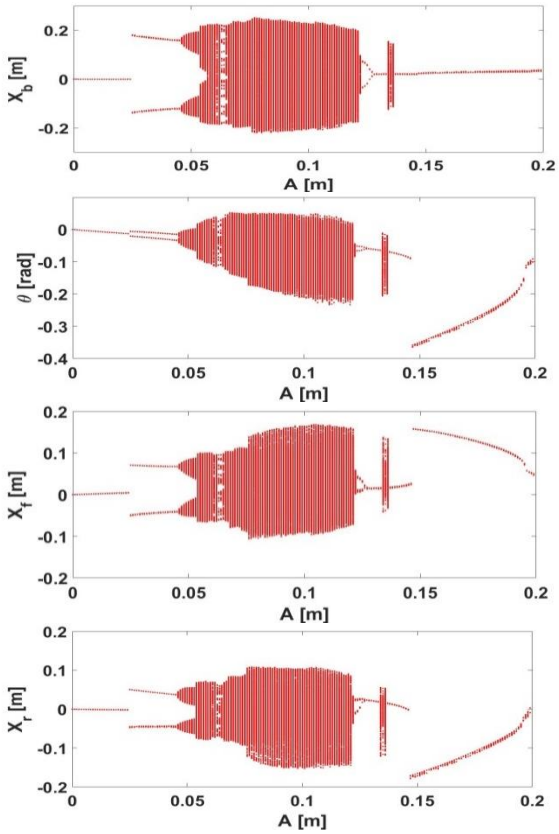

Figure 2: Bifurcation diagram of the displacement of system mode variables relative to the change of the control parameter of the road surface excitation amplitude

In order to study chaos in the system quantitatively, the max Lyapunov exponent diagram is used. Due to the strong influence of nonlinear systems with respect to the initial conditions, with a slight change in the initial conditions, its effect on the system dynamic behavior is investigated and the distance between the trajectories and consequently the rate of change of their distance is obtained as Lyapunov exponent (LE). Thus, LE for the variable x(t) can be defined as follows [9]:

$$\lambda_i = \lim_{t\to\infty}\frac{1}{t}\int_0^t E\left(x\left(\tau\right)\right)d\tau = \lim_{t\to\infty}\frac{1}{t}\ln\left|\frac{\delta x_i\left(t\right)}{\delta x_i\left(0\right)}\right| \quad (9)$$

, where, $E\left(x\left(\tau\right)\right)$ is the real part of eigenvalue related to Jacobi matrix the system. Chaotic systems have positive, negative and zero Lyapunov values, so that the positive LE indicates the divergence of the system's trajectories from the equilibrium point, its negative shows that the trajectories are approaching to the fixed points and the zero values of LE depicts the return of trajectories. In general, dissipated systems with stable and limited behavior have negative Lyapunov values. Figure (3) shows the Lyapunov exponent λ for the variables of system has been plotted according to Equation (9). Figure (4) indicates max Lyapunov exponent corresponding to the variable X_b. It is specified that if the nonlinear dynamics has at least one positive LE beside the negative value of the LE, as a result the system must have chaotic behavior and confirms the chaotic behavior in vehicle dynamics. In order to calculate the nonlinear system Lyapunov exponent, the Wolf algorithm was used [10].

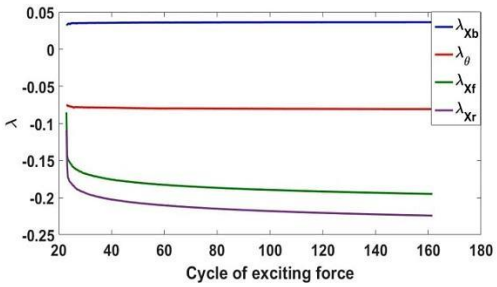

Figure 3: Lyapunov diagrams of system mode variables

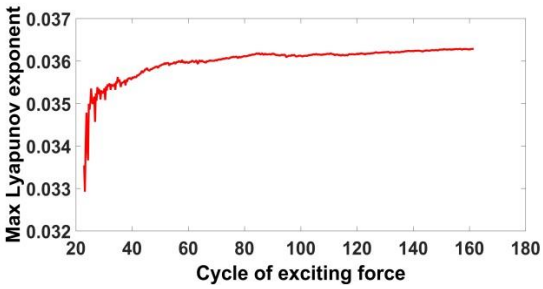

Figure 4: Max Lyapunov exponents of the mode variable x_b

Also, the results of Figures (5) to (7) depict that in the bifurcation shapes (a) in a specified interval, there is an irregular dynamic behavior with chaos as a consequence, in the shapes of Lyapunov (b), Max Lyapunov exponent is positive and confirms the chaotic behavior. Between the above two limits, the bifurcation diagram in Figure (a) shows a regular and periodic dynamic behavior, which accordingly, it is a negative Lyapunov exponent in Figure (b).

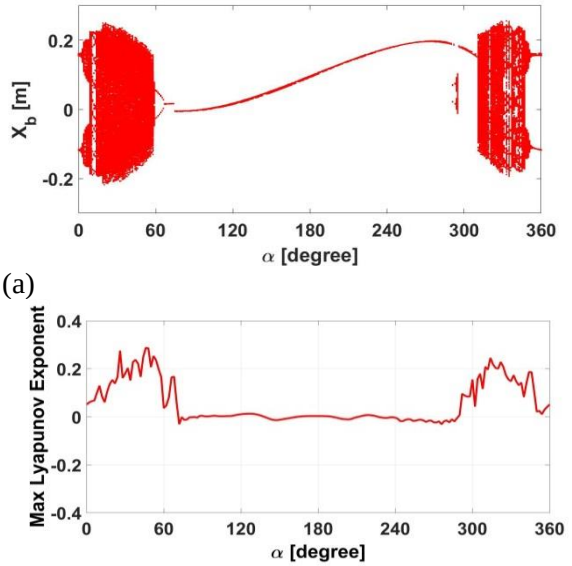

Figure 5: Max Lyapunov exponents (a) Bifurcation diagram in terms of phase angle control parameter, (b) Max Lyapunov exponent related to bifurcation diagram in terms of phase angle parameter

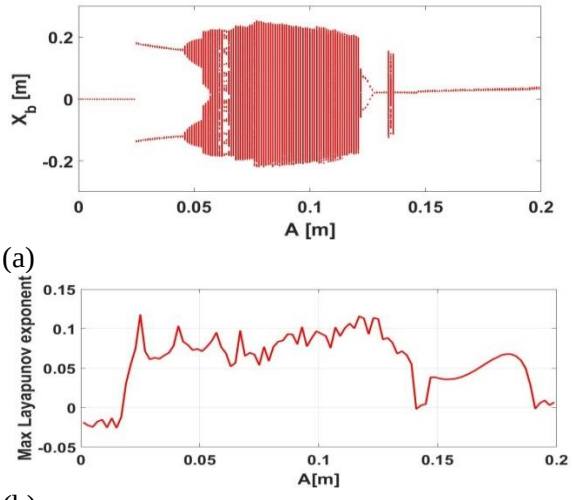

Figure 6: Max Lyapunov exponents (a) Bifurcation diagram in terms of control parameter of road surface excitation amplitude, (b) Max Lyapunov exponent of bifurcation diagram in terms of excitation amplitude parameter

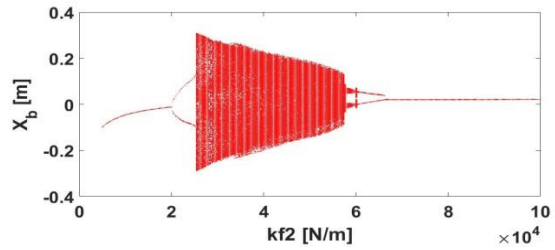

(a)

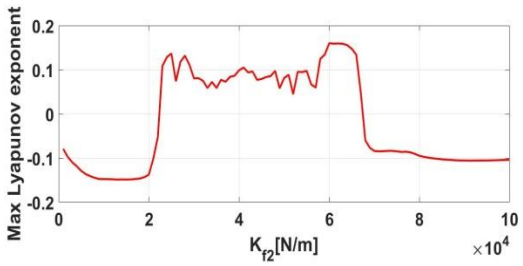

(b)

Figure 7: Max Lyapunov exponents (a) Bifurcation diagram according to the control parameter of the front suspension spring stiffness, (b) Max Lyapunov exponent related to the bifurcation diagram in terms of the front suspension spring stiffness

4. Chaos Control

In order to improve the control strategy including increasing stability, reducing settling time and eliminating chaos, at first, a nonlinear control algorithm is designed based on the development of SMC on the vehicle dynamic nonlinear system. Thus, a suitable control system can be obtained using the fast terminal sliding mode method and its positive features in addition to removing its important defect, which is chatting phenomenon [11-16].

4.1. Fast Terminal SMC

A dynamic system with following nonlinear mathematical model is considered:

$$x^{(n)} = f(x) + b(x)u \tag{10}$$

, where, $x = \left[x, \dot{x}, \ldots, x^{(n-1)}\right]$ is the system mode vector and *u* is controlled input.

In the fast-terminal SMC algorithm, in contrary to the sliding mode control scheme, the sliding surface is proposed as nonlinear exponentially and for this reason, it has a higher rate of convergence of system mode variables on the sliding surface. The sliding surface in the control of the fast terminal SMC is proposed as follows [13].

$$S = \dot{X}_1 + \alpha X_1 + \beta X_1^{q/p} = 0 \tag{11}$$

The control input function is designed by considering the above sliding surface ($S = 0$) equal to zero by as:

$$u = u_{eq} + u_d$$
$$u_{eq} = -b^{-1}(z).\left(a(z) + \sum_{k=0}^{n-2}\left(\alpha_k \ell_{A+Bu}^{n-k-1} s_k + \beta_k \ell_{A+Bu}^{n-k-1} s_k^{qk/pk}\right)\right) \tag{12}$$
$$u_d = -b^{-1}(z) K signs_{n-1}; \quad K > 0$$

In order to design a fast terminal SMC, the following sliding surfaces are considered as a combination of vertical displacement and velocity error of the rigid body as follows:

$$\begin{cases} S_1 = (\dot{x}_b - \dot{x}_{b_d}) + (x_b - x_{b_d}) + (x_b - x_{b_d})^{q/p} \\ S_2 = (\dot{\theta}_b - \dot{\theta}_{b_d}) + (\theta_b - \theta_{b_d}) + (\theta_b - \theta_{b_d})^{q/p} \end{cases} \tag{13}$$

The sliding condition is expressed as $\frac{dS}{dt} = -KS$ and the control coefficient K should be selected so that ensures the sliding conditions in order to place the system movement path on the sliding surface [9]. The dynamical model of a vehicle based on equations (5)-(8) is rewritten as matrix by the following relation:

$$\bar{M}\ddot{x} + \bar{C}\dot{x} + \bar{K}x = \bar{D}u \tag{14}$$

, where the vector of state varibles system including the vehicle dynamic variables along with the tire displacement of front and rear is defined as follows:

$$x = \left[x_b \;\; \theta \;\; x_f \;\; x_r \;\; x_{fd} \;\; x_{rd}\right]^T \tag{15}$$

Also

$$\bar{M} = \begin{bmatrix} M & 0 \\ 0 & 0 \end{bmatrix}_{6\times6}, \bar{C} = \begin{bmatrix} C & 0 \\ 0 & B \end{bmatrix}_{6\times6}, \bar{K} = \begin{bmatrix} K & 0 \\ 0 & A \end{bmatrix}_{6\times6}, \bar{D} = \begin{bmatrix} D \\ 0 \end{bmatrix}_{6\times2}, u = \begin{bmatrix} u_f \\ u_r \end{bmatrix}_{2\times1}$$

$$M=\begin{pmatrix} m_b & 0 & 0 & 0 \\ 0 & j & 0 & 0 \\ 0 & 0 & m_f & 0 \\ 0 & 0 & 0 & m_r \end{pmatrix},$$

$$C=\begin{pmatrix} C_{f2}+C_{r2} & L_fC_{f2}-L_rC_{r2} & -C_{f2} & -C_{r2} \\ L_fC_{f2}-L_rC_{r2} & L_f^2C_{f2}+L_r^2C_{r2} & -L_fC_{f2} & L_rC_{r2} \\ -C_{f2} & -L_fC_{f2} & C_{f1}+C_{f2} & 0 \\ -C_{r2} & L_rC_{r2} & 0 & C_{r1}+C_{r2} \end{pmatrix},$$

$$B=\begin{pmatrix} 0 & 0 \\ 0 & 0 \\ C_{f1} & 0 \\ 0 & C_{r1} \end{pmatrix}, \quad (16)$$

$$K=\begin{pmatrix} k_{f2}+k_{r2} & L_fk_{f2}-L_rk_{r2} & -k_{f2} & -k_{r2} \\ L_fk_{f2}-L_rk_{r2} & L_f^2k_{f2}+L_r^2k_{r2} & -L_fk_{f2} & L_rk_{r2} \\ -k_{f2} & -L_fk_{f2} & k_{f2}+k_{f1} & 0 \\ -k_{r2} & L_rk_{r2} & 0 & k_{r1}+k_{r2} \end{pmatrix},$$

$$A=\begin{pmatrix} 0 & 0 \\ 0 & 0 \\ k_{f1} & 0 \\ 0 & k_{r1} \end{pmatrix}, D=\begin{pmatrix} 1 & 1 \\ L_f & -L_r \\ -1 & 0 \\ 0 & -1 \end{pmatrix}$$

Finally, by writing Equation (15) as Equation (10) in which $f(x)=-\bar{M}^{-1}\bar{C}\dot{x}-\bar{M}^{-1}\bar{K}x$ and $b(x)=\bar{M}^{-1}\bar{D}$ are functions and by constituting it in Equation (12), the control input signal including the oil pressure applied to the front and rear hydraulic actuators is calculated as follows:

$$u=u_{eq}+u_d=\begin{bmatrix} u_f \\ u_r \end{bmatrix}=\begin{bmatrix} u_{eq_1}+u_{d_1} \\ u_{eq_2}+u_{d_2} \end{bmatrix}$$

$$=\begin{pmatrix} a(z)+ \\ -b^{-1}(z)\left(\sum_{k=1}^{8}\begin{pmatrix}\alpha_k\,\ell_{A+Bu}^{9-k}S_k+ \\ \beta_k\,\ell_{A+Bu}^{9-k}S_k^{qk/pk}\end{pmatrix}\right) \\ -b^{-1}(z)\ \ k\ \mathrm{sgn}(S_9) \end{pmatrix}$$

$$=\begin{pmatrix} -\left[\left(\nabla(\ell_f^9 x_b)\right)b(x)\right]^{-1}\times \\ \left[\begin{matrix}\ell_f^{10}\ x_b+ \\ \sum_{k=0}^{8}\begin{pmatrix}\alpha_k\,\ell_{[z_2,\ldots,z_{10},b(z)u]^T}^{9-k}S_k+ \\ \beta_k\,\ell_{[z_2,\ldots,z_{10},b(z)u]^T}^{9-k}S_k^{qk/pk}\end{pmatrix}\end{matrix}\right] \\ -\left[\nabla\left(\ell_f^9 x_b\right)\times b(x)\right]^{-1}k\ \mathrm{sgn}\,(S_9) \end{pmatrix} \quad (17)$$

According to the block diagram in Figure 8, the fuzzy inference system is able to estimate the fast terminal sliding mode control coefficients online. These coefficients are related to the values in the sliding surface including p and q and the control gain k according to equations (13) and (17), which should also be true in the sliding condition $\frac{dS}{dt}=-KS$.

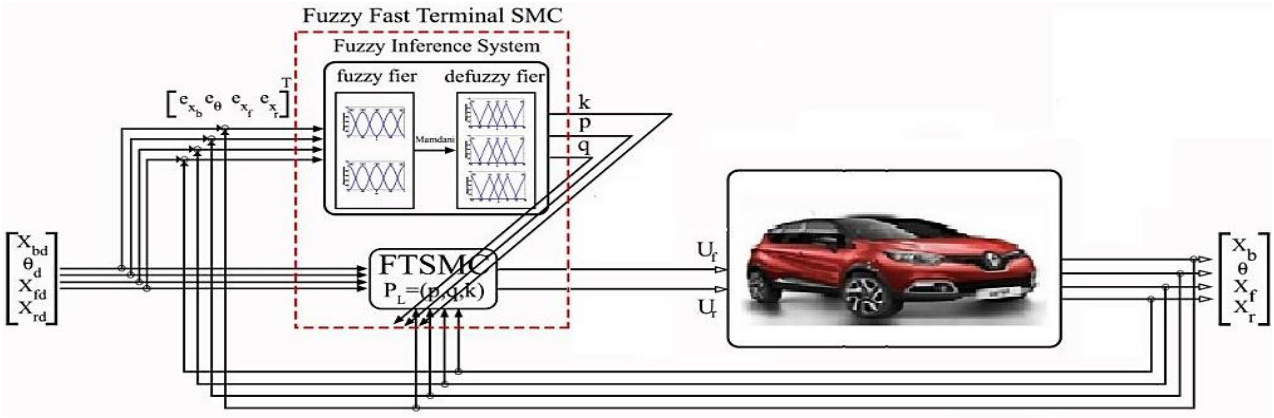

Figure 8: Fuzzy fast-terminal SMC block diagram of vehicle system

The general structure of fuzzy logic to estimate the best values for mentioned control coefficients is as follows.

Rule ith (R_i): If the error (e) is equal to F_{1i} and the derivative of the error (De) is equal F_{2i} then k will be equal to G_i.

Where, F_1 , F_2 and G are the membership type one functions for rule ith. Also, $F_1,F_2,G\subset[B-;S-;Z\,0;S+;B+]$ and the symbols are big negative, small negative, zero, small positive and big positive respectively. The base table of error-based fuzzy logic in the first row of the horizontal column equal to the error (e) and in the first vertical column equal

to the error derivative (De) for the fuzzy control inputs according to table 2 and 3. The selected fuzzy system is designed on the basis of Mamdani inference and the output of fuzzy is derived using the gravity center procedure.

Table 2: Fuzzy logic rules for K

De/e	B-	S-	Z0	S+	B+
B-	B-	B-	B-	S-	Z0
S-	B-	B-	S-	Z0	PS
Z0	B-	NS	Z0	S+	B+
S+	S-	Z0	S+	B+	B+
B+	Z0	S+	B+	B+	B+

Table 3: Fuzzy logic rules for p, q

De/e	B-	NS	ZO	PS	**B+**
B-	Z0	Z0	S+	S+	B+
S-	Z0	Z0	PS	B+	B+
Z0	Z0	S+	B+	B+	B+
S+	PS	B+	B+	B+	B+
B+	B+	B+	B+	B+	B+

4.2. Extended Pyragas controller

Control of chaos based on the properties of chaotic system brings the system responses to their desired value in addition to eliminating chaotic vibrations in less time with less energy. Therefore, the Pyragas based chaos control system is based on delay feedback for stabilization of alternating unstable orbits in which an UPO is estimated by mode variable with time delay without need for basic knowledge on the unstable orbit. In this control strategy, the feedback signal is based on the difference between linear mode and time delay, and the time delay constant is considered equal to the period of unstable orbits. Therefore, the control input signal is calculated simply as $u(t) = k[y(t-\tau) - y(t)]$, which τ is time delay and K is the control coefficient, which stability of periodic circuits is ensured by selecting its appropriate value [1, 2].

In order to improve the Pyragas control algorithm in fast stabilization, the system sliding mode nonlinear algorithm is used. In this way, if the system dynamics are defined as follows:

$$x^{(n)} = f_1(t,x) + f_2(t,x)u \tag{18}$$

, where x is the state variables vector, u is the control signal, the f_1 and f_2 are the functions with uncertainties and for u = 0, the system depict chaotic behavior. In this case, we first define the delay mode variable $\tilde{x}(t) = x(t-T)$ and it is obvious that the delay mode must satisfy Equation (18) as follows:

$$\tilde{x}^{(n)} = f_1(t-T,\tilde{x}) + f_2(t-T,\tilde{x})\tilde{u} \tag{19}$$

, where, $\tilde{u} = u(t-T)$. The system error dynamics with the difference of two equations (18) and (19) are obtained as follows:

$$\begin{aligned} x^{(n)} - \tilde{x}^{(n)} &= f_1(t,x) - f_1(t-T,\tilde{x}) \\ &\quad + f_2(t,x)u - f_2(t-T,\tilde{x})\tilde{u} \end{aligned} \tag{20}$$

Where $\underline{e} = \underline{x} - \underline{\tilde{x}}$ the error vector and the system error differential equation are expressed as follows:

$$\begin{aligned} e^{(n)} &= f_1(t,e+\tilde{x}) - f_1(t-T,\tilde{x}) \\ &\quad + f_2(t,e+\tilde{x})u - f_2(t-T,\tilde{x})\tilde{u} \end{aligned} \tag{21}$$

Therefore, the stability of a periodic unstable circuit in a chaos system according to Equation (20) leads to the stabilization of the error dynamics (21) that for increasing the system convergence rate to the stable balanced point, sliding mode resistive control algorithm has been used according to the system uncertainty and the sliding surface is defined as $S = \sum_{i=1}^{n+1} \alpha_i \hat{e}_i$ in which $\hat{e}_i(t) = \int_T^t e_i(s)ds = \int_T^t e^{(i-1)}(s)ds$ and $\alpha_i > 0$ to achieve a stable exponential dynamics to reach the system mode to the sliding mode, $S = 0$ must be constituted. In order to extract the control input *u* that the system trajectories cross the sliding surface intersection in a limited time, a definite positive function of Lyapunov is defined as $V = (1/2)S^2$ that is finally obtained by deriving from Lyapunov function and assuming $f_2(t,x) \rangle 0$ and simplifying the

calculations, the control input *u* is extracted as follows [3].

$$u = -\frac{1}{\alpha_n g_m(t,x)}.(\alpha_n \hat{f}(t,x) - \alpha_n \hat{f}(t-T,x) + \sum_{i=1}^{n} \alpha_i e_i + Ksign(S)) \quad (22)$$

Where the coefficient K should be true in the following inequality in order to satisfy the system Lyapunov stability condition:

$$K \geq (\frac{f_{2M}(t,x)}{f_{2m}(t,x)} - 1) \times \left| \sum_{i=1}^{n} \alpha_i e_i + \alpha_n f_1(t,x) - \alpha_n f_1(t-T,x) \right| + \alpha_n F(t,x) + \alpha_n F(t-T,x) + f_{2M}(t-T,x)|\tilde{u}| + \theta \quad (23)$$

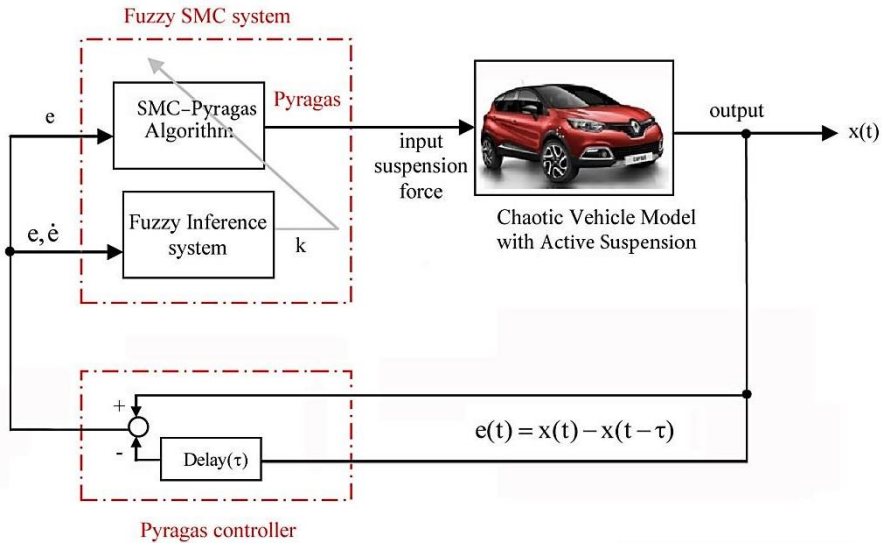

Figure 9: Delayed feedback Fuzzy-sliding control block diagram system

In order to concentrate a chaos controller on the chaotic dynamics, active suspension eliminate the chaotic vibrations along with improving system behavior in the shortest possible time and best energy consumption, a delay feedback controller modified by SMC algorithm is used to control the system appropriately according to the chaotic properties. Also, the structure of the control system has been improved by integrating the fuzzy logic system in the sliding delay feedback control algorithm by calculating the control gains online. In this way, the control coefficient, which was previously estimated by trial and error, is determined here using a fuzzy inference system accurately and according to each specific dynamic maneuver that improves the designed control system. According to the control block diagram in Figure 9, the pressure control system provides the required oil for active suspension hydraulic actuator, as a result the stabilizing forces on the vertical dynamics of the vehicle are applied to the chassis by these actuators. In the delayed feedback chaos control system developed with sliding mode, as the system dynamics reach sliding mode, the periodic unstable orbits are stabilized and the chaos is eliminated. In designing the mentioned control system, first, it is important to calculate the control coefficient K that its value must be true in Equation (22) and then eliminate the effect of sliding the system's trajectories around the sliding surface while generating control input due to sliding mode that prevents chattering phenomenon. For this purpose, fuzzy inference is used for online and accurate estimation of the control coefficient K, and finally, the delayed feedback fuzzy-sliding controller stabilizes the system alternating orbits.

In order to estimate the best control coefficient of the sliding Pyragas system by fuzzy inference, with the help of fuzzy system inputs including error and its derivative according to the dynamics of the delayed feedback stabilization, the appropriate value K is calculated in the sliding mode system

according to the fuzzy rules mentioned in the previous control section.

Figures (10-13) show the comparison of the behavior of both extended Pyragas and fast terminal fuzzy-sliding controllers with open loop system for system variables.

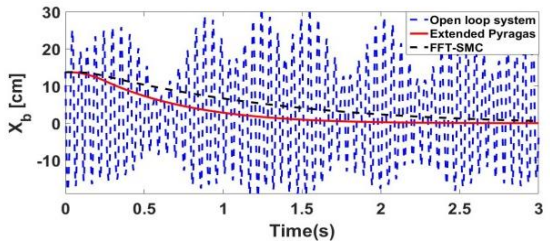

Figure 10: Comparison of vertical displacement of vehicle body under fast-terminal fuzzy-sliding controller with extended Pyragas controller

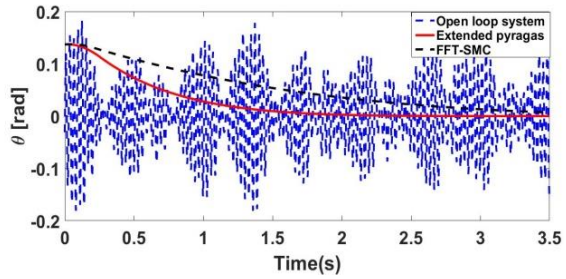

Figure 11: Comparison of angular displacement of the vehicle body under the fast terminal fuzzy-sliding controller with the extended Pyragas controller

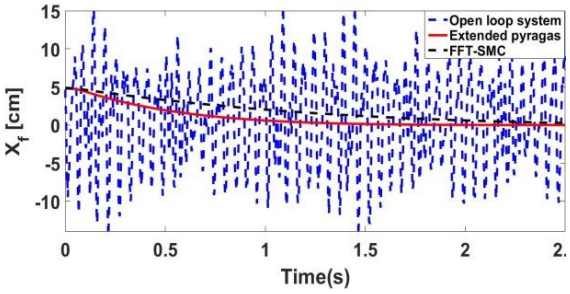

Figure 12: Comparison of displacement of front wheel under fast terminal fuzzy-sliding controller with extended Pyragas controller

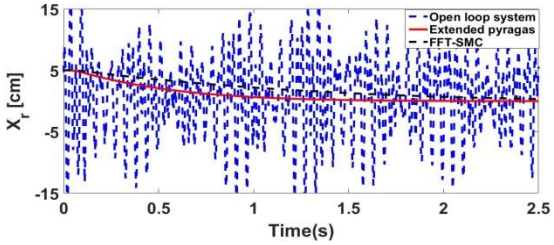

Figure 13: Comparison of displacement of rear wheel under fast terminal fuzzy-sliding controller with extended Pyragas controller

In order to consider the performance of the control system actuators, the equivalent damping force related to the active vehicle suspension system is analyzed as control input signals. A comparison of the dynamic behavior of the forces exerted by the active front and rear suspension on the vehicle chassis, including the force variables FC_{sf} and FC_{sr} under the controllers is shown in Figure 14 that depict the vehicle stabilization after converging the control system in appropriate time. As it has been specified, with the application of the extended Pyragas controller, significant reduction is seen in amplitude of the control signals, while reducing consumption of energy and completely eliminates the problem of saturation in the suspension operators. Also, the settling time is less than the fast terminal fuzzy-sliding controller that leads to faster stabilization of the system.

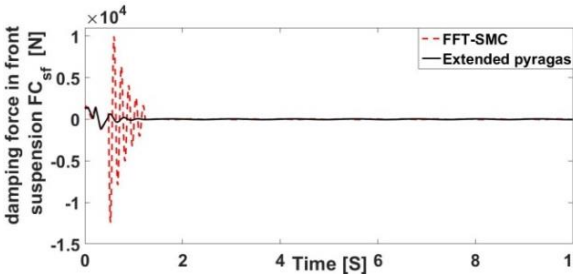

(a)

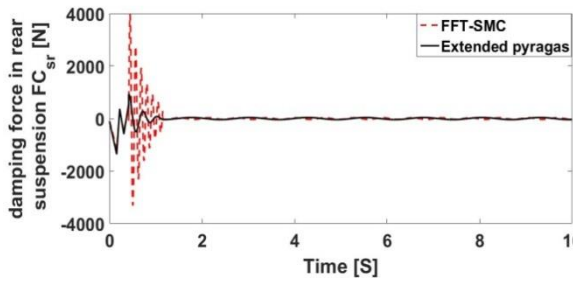

(b)

Figure 14: Comparison of damping force equivalent to active suspension under the application of fast-terminal sliding fuzzy controllers and extended Pyragas, (a) active front suspension, (b) active rear suspension

5. Conclusion

The chaotic dynamics of the vehicle model is numerically investigated and control of chaos is designed for the system in this paper. Dynamical model is derived via the Newton-Euler relations and simulated by the fourth-

order Runge-Kutta. Bifurcation diagrams and max Lyapunov exponent are used to confirm occurrence of chaos in the system. Then, by presenting a new fuzzy fast-terminal SMC method, chaotic irregular vibrations are eliminated and the dynamical system can be stabilized. In order to control the system and eliminate the chaotic vibrations, control of chaos is used based on the delayed feedback developed by the SMC algorithm in the active suspension system. The comparison of the results of this article with the reference [9] showed reduction of settling time in the responses by 10% along with the elimination of major overshoots in the dynamic system responses. Also, the comparison of the control signals of this paper with the reference [9] indicated a significant reduction in overshoot in the control input responses while reducing consumption of energy, eliminates the saturation problem in the suspension actuators.

6. Notion

Xb	Vertical displacement of main body Mb, (m)
θ	Displacement of body angles Mb, (rad)
Xf	Displacement of the front tire Mf, (m)
Xr	Displacement of rear tire Mr, (m)
Xfd	Induction displacement to the front tire
Xrd	Induction displacement to rear tire
Cf1	damping coefficient of Front tire, kg/s
Cr1	damping coefficient of Rear tire, kg/s
Cf2	damping coefficient of Front suspension, kg/s
Cr2	damping coefficient of Rear suspension, kg/s
Mb	Vehicle body mass
J	Moment of inertia of the vehicle body
M	Rubber mass
n1, *n2*	Nonlinear coefficient of suspension and tire springs
L	Distance of the vehicle mass center to the suspension system
f	Frequency of excitation force, Hz
α	Delay in displacement applied from road roughness to front and rear tires
λ	Lyapanov exponent
f	Front suspension
r	Rear suspension

References:

[1] K. Pyragas, "Continuous Control of Chaos by Self- Controlling Feedback." Physics letters A, Vol. 170, pp. 421-428, (1992).

[2] K. Pyragas, and E.A. Tamas, "Experimental Control of Chaos by Delayed Self-Controlling Feedback", Phys. Lett. A, Vol. 180, pp. 99–102 (1993).

[3] H. Salarieh and A. Alasty, "Chaos Control in Uncertain Dynamical Systems Using Nonlinear Delayed Feedback" Chaos, Solitons & Fractals, Vol. 41, pp. 67-71, (2009).

[4] F. Pashaei and M. Abtahi, "Chaotic Analysis and Chaos Control of a Lateral Dynamics Vehicle Based on the Nonlinear Poincare Map with Fuzzy Controller" Automotive Science and Engineering, Vol. 11, No.4, (2021) , 3693-3700.

[5] B. Sepehri, A. Hemati, "Active Suspension Vibration Control Using Linear H-Infinity and Optimal Control" Automotive Science and Engineering,Vol.4,Issue3 (9-2014).

[6] M. Salehpour, A. Bagheri, "Pareto optimization of a nonlinear vehicle model using multi-objective differential evolution algorithm with fuzzy inference-based adaptive mutation factor(MODE-FM)" Automotive Science and Engineering, Vol. 11, No.3, (2021) , 3594-3613.

[7] Q. Zhu, M. Ishitobi, Chaos and bifurcations in a nonlinear vehicle model, Journal of Sound and Vibration, 275(3-5) (2004) 1136-1146.

[8] S.M. Abtahi, "Chaotic Study and Chaos Control in a Half-Vehicle Model with Semi-Active Suspension Using Discrete Optimal Ott–Grebogi–Yorke Method", Journal of Multi-body Dynamics, Vol. 231, pp. 148–155 (2017).

[9] S.M. Abtahi, 2019. Suppression of chaotic vibrations in suspension system of vehicle dynamics using chattering-free optimal sliding mode control, Journal of the Brazilian Society of Mechanical Sciences and Engineering, 41(5) 210.

[10] A. Wolf, J. B. Swift, H. L. Swinney, J. A. Vastano, 1985. Determining lyapunov exponents from a time series, Physica D, Vol 16, pp. 285-317.

[11] S. Laghrouche, F. Plestan, A. Glumineau, Higher order sliding mode control based on integral sliding mode, Automatica, 43(3) (2007) 531-537.

[12] H. Li, X. Liao, C. Li, C. Li, Chaos control and synchronization via a novel chatter free sliding mode control strategy, Neurocomputing, 74(17) (2011) 3212-3222.

[13] H.Wang, Z.-Z. Han, Q.-Y. Xie, W. Zhang, Finite-time chaos control via nonsingular terminal sliding mode control, Communications in Nonlinear Science and Numerical Simulation, 14(6) (2009) 2728-2733.

[14] S. Dadras, H. R. Momeni, V.J. Majd, Sliding mode control for uncertain new chaotic dynamical system, Chaos, Solitons & Fractals, 41(4) (2009) 1857-1862.

[15] M. R. Faieghi, H. Delavari, D. Baleanu, Control of an uncertain fractional-order Liu system via fuzzy fractional-order sliding mode control, Journal of Vibration and Control, 18(9) (2012) 1366-1374.

[16] Y. Hong, G. Yang, D. Cheng, S. Spurgeon, A new approach to terminal sliding mode control design, Asian Journal of Control, 7(2) (2005) 177-181.